the plant journal

SEB SOCIETY FOR EXPERIMENTAL BIOLOGY

The Plant Journal (2019) **100,** 221–236 doi: 10.1111/tpj.14459

Root endodermal barrier system contributes to defence against plant-parasitic cyst and root-knot nematodes

Julia Holbein[1], Rochus B. Franke[2], Peter Marhavý[3], Satoshi Fujita[3,†], Mirosława Górecka[4], Mirosław Sobczak[4], Niko Geldner[3], Lukas Schreiber[2], Florian M. W. Grundler[1] and Shahid Siddique[1,5,*]

[1]INRES – Molecular Phytomedicine, Rheinische Friedrich-Wilhelms-University of Bonn, Karlrobert-Kreiten-Straße 13, 53115, Bonn, Germany,

[2]IZMB – Ecophysiology, Rheinische Friedrich-Wilhelms-University of Bonn, Kirschallee 1, 53115, Bonn, Germany,

[3]Department of Plant Molecular Biology, University of Lausanne, 1015 Lausanne, Switzerland,

[4]Department of Botany, Warsaw University of Life Sciences (SGGW), Nowoursynowska 159, 02-787, Warsaw, Poland, and

[5]Department of Entomology and Nematology, University of California, Davis, One Shields Ave., Davis, CA, 95616, USA

Received 7 July 2018; revised 2 July 2019; accepted 9 July 2019; published online 19 July 2019.

*For correspondence (e-mail ssiddique@ucdavis.edu).

†Present address: National Institute for Genetics (NIG), Yata 1111, Mishima, Shizuoka, 411-8540, Japan

SUMMARY

Plant-parasitic nematodes (PPNs) cause tremendous yield losses worldwide in almost all economically important crops. The agriculturally most important PPNs belong to a small group of root-infecting sedentary endoparasites that includes cyst and root-knot nematodes. Both cyst and root-knot nematodes induce specialized long-term feeding structures in root vasculature from which they obtain their nutrients. A specialized cell layer in roots called the endodermis, which has cell walls reinforced with suberin deposits and a lignin-based Casparian strip (CS), protects the vascular cylinder against abiotic and biotic threats. To date, the role of the endodermis, and especially of suberin and the CS, during plant–nematode interactions was largely unknown. Here, we analyzed the role of suberin and CS during interaction between Arabidopsis plants and two sedentary root-parasitic nematode species, the cyst nematode *Heterodera schachtii* and the root-knot nematode *Meloidogyne incognita*. We found that nematode infection damages the endodermis leading to the activation of suberin biosynthesis genes at nematode infection sites. Although feeding sites induced by both cyst and root-knot nematodes are surrounded by endodermis during early stages of infection, the endodermis is degraded during later stages of feeding site development, indicating periderm formation or ectopic suberization of adjacent tissue. Chemical suberin analysis showed a characteristic suberin composition resembling peridermal suberin in nematode-infected tissue. Notably, infection assays using Arabidopsis lines with CS defects and impaired compensatory suberization, revealed that the CS and suberization impact nematode infectivity and feeding site size. Taken together, our work establishes the role of the endodermal barrier system in defence against a soil-borne pathogen.

Keywords: nematodes, endodermis, Casparian strip, apoplastic barriers, suberin, plant.

Linked article: This paper is the subject of a Research Highlight article. To view this Research Highlight article visit https://doi.org/10.1111/tpj.14540.

INTRODUCTION

Plant-parasitic nematodes (PPNs) cause tremendous yield losses in many crops, which are estimated to a total over US$80 billion per year (Nicol *et al.*, 2011). Different species of PPNs infect different plant tissues, including flowers, stems, and leaves. However, the most complex and economically important group of PPNs comprises root-infecting sedentary endoparasites that includes cyst nematodes (CNs; *Heterodera* spp. and *Globodera* spp.) and root-knot nematodes (RKNs; *Meloidogyne* spp.). While both CNs and RKNs have a sedentary lifestyle, they differ in their migration and feeding characteristics. Infective second-stage juveniles (J2s) of CNs enter the root at any location and have developed mechanisms to cross the cortex tissue (including endodermis) directly to reach the vascular cylinder (Marhavy *et al.*, 2019) where their feeding site is induced. RKNs J2s predominantly enter the root close to the tip and then move towards the apical

meristematic region, making a U-turn to enter the vascular cylinder without crossing the differentiated endodermis (Sijmons *et al.*, 1991; Wyss *et al.*, 1992). CNs J2s are destructive, moving intracellularly and piercing cells with their stylets. In contrast, RKNs J2s cause comparatively little damage, as they move intercellularly through root tissue (Sijmons *et al.*, 1991; Wyss *et al.*, 1992; Shah *et al.*, 2017).

Within the central vasculature, the J2s of both nematode groups induce characteristic nurse cell systems. The induction of these feeding sites requires cellular reprogramming, which is achieved by a cocktail of proteinaceous and non-proteinaceous compounds secreted by the J2s into the initial feeding cell. These secretions induce profound ultrastructural and physiological changes in both the initial feeding cell and adjoining tissue (Siddique *et al.*, 2015; Juvale and Baum, 2018; Smant *et al.*, 2018). CNs form syncytia by locally dissolving cell walls and fusing the protoplasts of neighbouring cells into single entities (Golinowski *et al.*, 1996; Sobczak *et al.*, 1997). RKNs induce the formation of several adjacent hypertrophied giant cells. For RKNs, the divisions of the parenchymatous vascular cylinder cells surrounding the nematode and the hypertrophy of giant cells lead to the formation of typical galls, which are a symptom of infection. Both types of nematode feeding sites share the following cellular features: dense cytoplasm, multiple nuclei, small vacuoles, proliferation of plastids, mitochondria, and endoplasmic reticulum structures, and modified cell walls. The feeding sites are highly metabolically active and are the sole nutrient source for the sedentary nematodes (Kyndt *et al.*, 2013; Siddique and Grundler, 2015, 2018). A few hours after the induction of a syncytium or giant cell, the nematodes begin to withdraw nutrients from the modified plant cells (Wyss and Grundler, 1992; Wyss *et al.*, 1992).

A relatively little studied aspect of plant defence against nematodes is the protective function of preformed cell wall polymers, such as suberin and lignin, in the endodermis, which encloses the central vasculature in roots (Holbein *et al.*, 2016). Both suberin and lignin confer the apoplastic barrier properties of the endodermis. Lignin-based cell wall reinforcements are deposited in radial and transversal cell walls that encircle the cell as the Casparian strip (CS). Second-stage endodermis differentiation proceeds with the suberization of entire cell walls. Whereas suberin limits transmembrane transport by establishing a barrier for uptake from the apoplast into the cell interior (Barberon *et al.*, 2016), the CS seals the apoplastic pathway in and out of the endodermis, therefore preventing diffusion of toxins and loss of nutrients (Naseer *et al.*, 2012).

The periderm is formed during later stages of root development and replaces the endodermis as a sealing tissue. Unlike the endodermis, the periderm is not equipped with CSs and consequently does not function as a selective barrier. Instead the periderm is fully suberized. Studies carried out so far showed a rather fast transition from endodermal to peridermal protection in Arabidopsis roots and hypocotyls (Dolan and Roberts, 1995; Wunderling *et al.*, 2018). To date, only a few studies have indicated a role for endodermal/peridermal suberin and lignin in the resistance response to nematode infection (Balhadère and Evans, 1995; Valette *et al.*, 1998).

Many enzymes involved in suberin biosynthesis have been identified, including a fatty acid ω-hydroxylase (CYP86A1/HORST, hydroxylase of root suberized tissue), a β-ketoacyl-CoA synthase (KCS2/DAISY, docosanoic acid synthase), an acyl-CoA:glycerol-3-phosphate acyltransferase (GPAT5), and a hydroxy-cinnamoyl-CoA transferase (ASFT, aliphatic suberin feruloyl transferase) (Beisson *et al.*, 2007; Höfer *et al.*, 2008; Compagnon *et al.*, 2009; Franke *et al.*, 2009; Gou *et al.*, 2009; Molina *et al.*, 2009). The expression pattern of promoter:GUS fusion of *CYP86A1*, *ASFT*, and *GPAT5* in transgenic Arabidopsis overlaps with suberin deposition in the endodermis (Naseer *et al.*, 2012). Furthermore, the transcriptional reporter *GPAT5:mCitrine-SYP122* has been shown to act as a marker for suberization (Barberon *et al.*, 2016).

The mechanism of CS formation is relatively well described (Roppolo *et al.*, 2011; Lee *et al.*, 2013). A family of transmembrane proteins called CASPs (Casparian Strip Domain Proteins) drives CS formation by accumulating at the appropriate membrane locations (Roppolo *et al.*, 2011). The expression pattern of the reporter *pCASP1:NLS3xmVenus* was shown to coincide with CS formation during root development (Vermeer *et al.*, 2014; Barberon *et al.*, 2016). CS establishment also depends on the dirigent domain-containing protein ESB1 (ENHANCED SUBERIN 1). ESB1 is localized at the CS and mediates lignin deposition and stabilization (Hosmani *et al.*, 2013). Another protein important for localizing CASPs is the receptor-like kinase SGN3 (SCHENGEN 3), which is responsible for forming CASP complexes in the membrane (Pfister *et al.*, 2014). Previous studies have shown that ectopic depositions of suberin compensates for CS defects (reviewed in Barberon, 2017 and Doblas *et al.*, 2017a).

The identification of genes and the development of appropriate marker lines during the last few years has created new opportunities to analyze suberization and CS formation in Arabidopsis. An *in vitro* system comprising Arabidopsis, the beet CN *Heterodera schachtii*, and the RKN *Meloidogyne incognita* provides optimal conditions to study the cellular and molecular aspects of plant–nematode interactions. Making use of this system, we studied the role of suberin and CS in plant–nematode interactions (Sijmons *et al.*, 1991). Our results indicated an important role for endodermal sealing in nematode development.

RESULTS

Transcripts of suberin biosynthesis-related genes are increased at sites of nematode infection

We surveyed transcriptome data of nematode infection sites available in NEMATIC (NEMatode–Arabidopsis Transcriptomic Interaction Compendium) to gain insight into the expression pattern of a number of suberin- and CS-related genes (Table S1) (Cabrera *et al.*, 2014). We found that the overall expression of these genes was not altered in *M. incognita* galls from 3 to 21 days after inoculation (dai). However, the transcript levels of a few suberin biosynthesis genes (*ASFT*, *KCS2*/*DAISY* and *FAR4*) were reduced in giant cells at 3 dai (Barcala *et al.*, 2010). In contrast, the transcript levels of most suberin- and CS-related genes were found to be significantly reduced in syncytia induced by *H. schachtii* at 5 and 15 dai (Szakasits *et al.*, 2009). The transcriptome analysis by Szakasits *et al.* (2009) was conducted on RNA isolated from micro-aspirated syncytium protoplasts excluding the root tissue surrounding syncytia. As suberin- and CS-related genes are almost exclusively expressed in the endodermis, we hypothesized that the strong reduction in transcripts of suberin- and CS-related genes reported in Szakasits *et al.* (2009) might be due to the exclusion of surrounding root tissue. Therefore, to investigate whether the selected genes are differentially expressed in infected tissue, we dissected root segments containing *H. schachtii* infection sites and quantified gene expression in these segments (Figure 1). We found that transcript abundance of *ESB1*, *CASP1* and *SGN3* was reduced, whereas transcript abundance of *CYP86A1*, *KCS2*/*DAISY*, *CYP86B1*, *FAR4* (encoding fatty acyl reductase4), *FAR5* (encoding fatty acyl reductase5), and *GPAT5* was increased in root segments containing syncytia. Furthermore, although not statistically significant, *ASFT*, *FAR1* (encoding fatty acyl reductase 1), *KCS2* (ß-ketoacyl-CoA synthase 2), and LACS (long-chain acyl-CoA synthetase) showed a slight increase in transcript abundance. Taken together, many suberin biosynthesis genes showed increased expression in infection sites, while expression of genes involved in CS formation was decreased.

Suberin biosynthesis genes are expressed in tissue surrounding nematode infection sites

To determine the spatiotemporal patterns of expression of suberin biosynthesis- and CS formation-related genes during plant–nematode interactions, we analyzed previously described promoter:reporter lines at three different time points after inoculation (3, 5, and 10 dai) with *H. schachtii* or *M. incognita*. The activity of *pCYP86A1:GUS* and *pGPAT5:mCitrine-SYP122* was used as an indicator of suberin biosynthesis (Höfer *et al.*, 2008; Naseer *et al.*, 2012; Barberon *et al.*, 2016). Expression of *pELTP:mCitrine-SYP122* was used as a marker for endodermis and *pCASP1:NLS3xmVenus* served as a marker of CS formation (Vermeer *et al.*, 2014).

In lines expressing *pCYP86A1:GUS*, we found that most infection sites exhibited GUS staining upon *H. schachtii* infection. The staining appeared slightly more intense in the infected area as compared with the surrounding tissue at 3 dai (Figure S1a). At 5 and 10 dai, single cells were stained in the cell layer surrounding syncytium, producing a highly localized, patchy pattern. At 3 dai with *M. incognita*, *pCYP86A1:GUS* expression was observed close to root swellings appearing in root tips (Figure S1b). However, at 5 and 10 dai, intense GUS staining was detected throughout the gall tissue (Figure S1b). To confirm that the activity of *pCYP86A1:GUS* was localized to endodermal tissue, cross-sections of feeding sites were prepared at 5 dai (Figure S1c). No GUS staining was observed in the cortical parenchyma, however specific staining was present in the tissue surrounding feeding sites induced by CN or RKN. Occasionally, GUS staining was also observed in the central vasculature, most likely due to leakage of excessive staining from the endodermis into the vasculature.

Previous studies have shown that CS defects lead to the escape of CASPARIAN STRIP INTEGRITY FACTORS (CIF) peptides from the stele, leading to the continuous activation of the SGN3–SGN1 signalling module, causing lignification/suberization of the defected tissue and therefore sealing the endodermal barrier (Alassimone *et al.*, 2016; Doblas *et al.*, 2017b). *SGN3* loss-of-function leads to strong

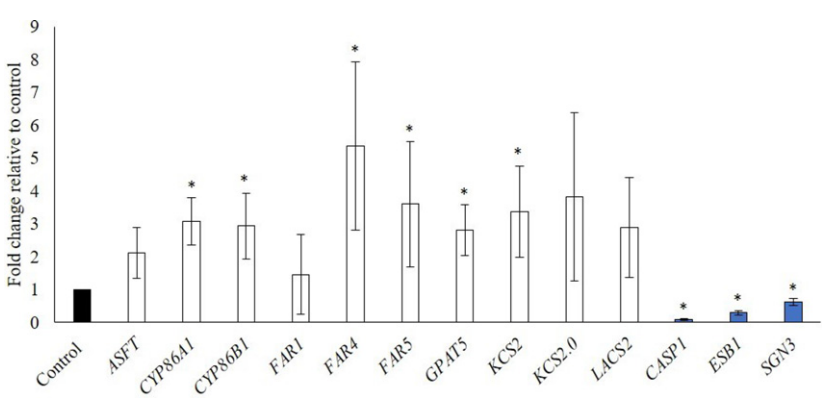

Figure 1. Expression of suberin- and Casparian strip (CS)-related genes in root segments containing syncytia. 10–12-day old Arabidopsis plants were inoculated with *H. schachtii* J2s and gene expression in dissected root tissue containing syncytia at 10 days after inoculation (dai) was compared with uninfected roots as analyzed via qPCR. White bars, suberin biosynthesis-related genes; blue bars, CS formation-related genes. Bars, means ± SD; asterisks, statistically significant fold change relative to the control (*t*-test, $P < 0.05$); $n = 4$.

CS defects without deposition of compensatory suberin (Hosmani *et al.*, 2013). Based on activation of suberin biosynthesis-related genes, we hypothesized that nematode damage may as well cause leakage of CIF from the stele, leading to the enhanced suberization as a part of a CIF/SGN3-dependent signalling cascade for CS integrity maintenance. To test this hypothesis, we analyzed the suberization of infected tissues using *pGPAT5:mCitrine-SYP122* expression in Col-0 and *sgn3*. We observed a clear expression of *pGPAT5:mCitrine-SYP122* in cell layer surrounding the nematode feeding sites induced by CN or RKN (Figures 2 and 3). We found that expression of *pGPAT5:mCitrine-SYP122* was only slightly reduced in the *sgn3* background upon CN infection. However, expression of *pGPAT5:mCitrine-SYP122* appeared to be reduced strongly at all time points in RKN infected tissues as compared with CN (Figures 2c,d and 3c,d).

We next monitored the fate of endodermis upon infection *with H. schachtii* or *M. incognita* using the expression of *pELTP:mCitrine-SYP122*. In uninfected roots, we found a clear expression of *pELTP:mCitrine-SYP122* at all time points (Figure 4a,c). Upon infection, we observed expression of *pELTP:mCitrine-SYP122* in the cell layer around syncytia or galls at 3 dai (Figure 4b,d). However, beginning at 5 dai, we observed a decrease in expression of *pELTP:mCitrine-SYP122* at the infection site as compared with adjacent non-infected tissues, indicating the degradation of endodermis (Figure 4b,d). Interestingly, the extent of endodermal degradation (as indicated by lack of *pELTP:mCitrine-SYP122* expression) appeared to be particularly strong in regions infected by CN as compared with RKN. At 10 dai, expression of *pELTP:mCitrine-SYP122* was absent in infected, as well as in non-infected, tissues indicating complete degradation of endodermis (Figure 4b,d). For *pCASP1:NLS3xmVenus*, the punctate expression pattern was not detectable at 5 and 10 dai, although a few sites at 3 dai in young root samples showed weak expression at the infection sites for both syncytia and galls (Figure S2).

Taken together, these findings showed that both syncytia and galls are surrounded by endodermis during early stages of infection and feeding site development. However, the endodermis becomes degraded between 3 and 5 dai, this change indicates periderm formation or ectopic suberization. Regardless of the identity of the tissue, we found

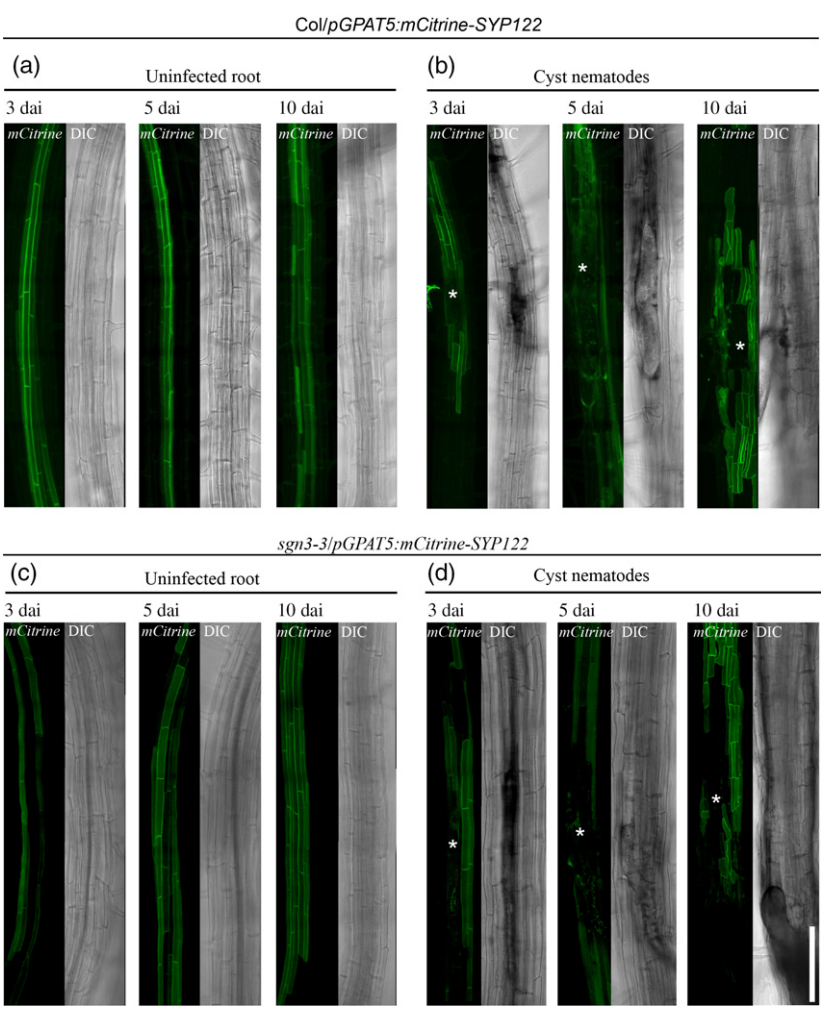

Figure 2. 3D Tile-scan (xyz) maximum projection images monitoring *pGPAT5:mCitrine-SYP122* in Col-0 (a, b) and *sgn3* (c, d) background upon cyst nematode (CN) infection. Here, 10–12-day old Arabidopsis plants were inoculated with second-stage juveniles (J2s) of *Heterodera schachtii* and images were taken at 3, 5 and 10 days after inoculation (dai). Asterisks indicate cyst nematode-induced feeding site (syncytium). Representative images are shown. Scale bar, 200 μm.

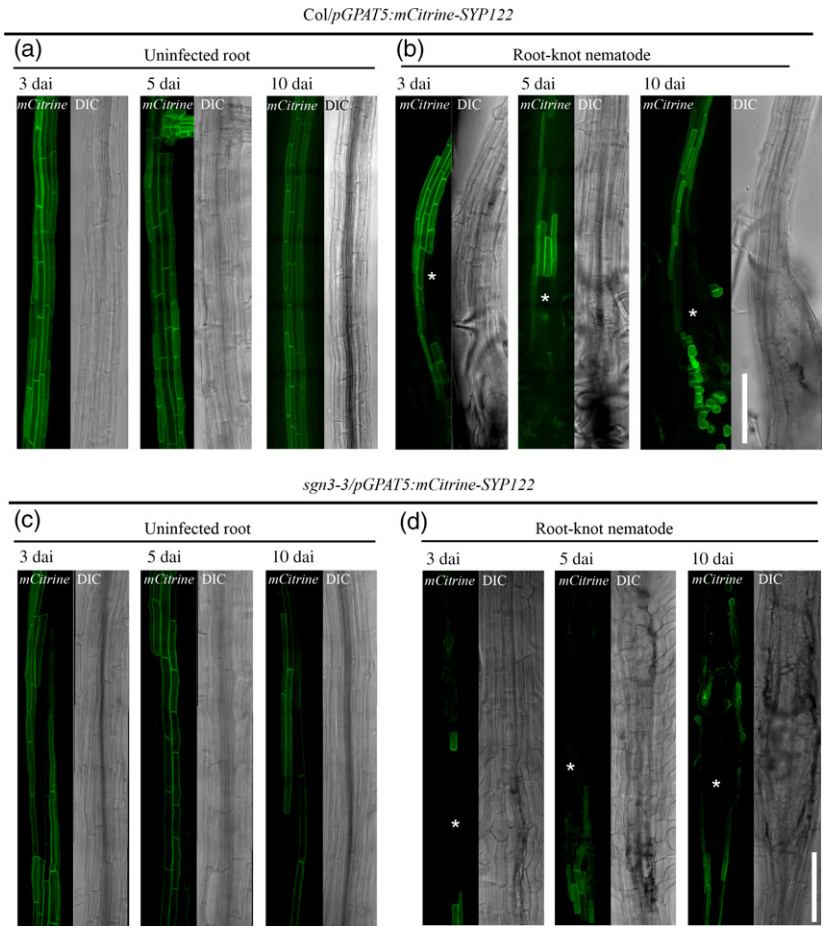

Figure 3. 3D Tile-scan (xyz) maximum projection images monitoring *pGPAT5:mCitrine-SYP122* in Col-0 (a, b) and *sgn3* (c, d) background upon root-knot nematode (RKN) infection. Here, 10-12-day old Arabidopsis plants were inoculated with second-stage juveniles (J2s) of *Meloidogyne incognita* and images were taken at 3, 5 and 10 days after inoculation (dai). Asterisks indicate root-knot nematode-induced feeding site (galls). Representative images are shown. Scale bar, 200 μm.

that suberin biosynthesis genes are activated in cells surrounding the infection sites of both CNs and RKNs.

Periderm is formed during the later stages of infection

Some previous studies have mentioned degradation of the endodermis and the presence of periderm-like tissue around syncytia (Golinowski *et al.*, 1996; Sobczak *et al.*, 1997; Radakovic *et al.*, 2018; Różańska *et al.*, 2018). To analyze this anatomical problem in more detail, we conducted serial sectioning of samples with nematode infection sites at 3, 5 and 10 dai (Figures 3 and 5). Our examinations confirmed results provided by Wunderling *et al.* (2018) who showed that in non-infected roots, endodermis with relatively clearly recognizable CSs (Figure S3a) starts to degenerate when primary xylem bundles are fully differentiated and pericyclic cells start to divide (Figure S3b). Based on the numbers of primary xylem vessels and the presence of secondary xylem vessels, we were able to identify basipetal and acropetal ends of syncytia induced by *H. schachtii* (Figure 5). The endodermis was well preserved at the basipetal region of infection sites containing syncytia at 3 dai (Figure 5a,b). But it was partially destroyed or sometimes even hardly recognizable along syncytia and close to the acropetal region behind the syncytium (Figure 5c–f). In the same samples, cellular divisions were absent in the pericycle located at the basipetal region of infection sites (Figure 5a), but occurred along the syncytium, except in the region next to the nematode head where most cells were destroyed, and at the acropetal part of the infection site (Figure 5b–f). In samples from infection sites collected at 5 dai, the endodermis was found at both regions but only when the syncytium and dividing pericyclic cells were absent on sections (Figure 5g,l). When the syncytium appeared on sections it was surrounded by dividing pericycle, and degraded and detaching endodermal, cortical parenchyma and epidermal cells (Figure 5h–k). Transmission electron microscopy observations confirmed the degradation of endodermis around syncytia (Figure S3c) and formation of the periderm from dividing pericycle cells (Figure S3d). The cells in the outer layer of the periderm started to differentiate into dead phellem (cork) cells with suberized cell walls (Wunderling *et al.*, 2018). No functional endodermal cells were found in samples collected at 10 dai (Figure 5m–r). Sections taken at basipetal and acropetal regions of samples contained roots that were at early stages of secondary thickening and had well developed periderm. It is worth to note that the number of cells forming the periderm and the diameter of the root at distal regions of

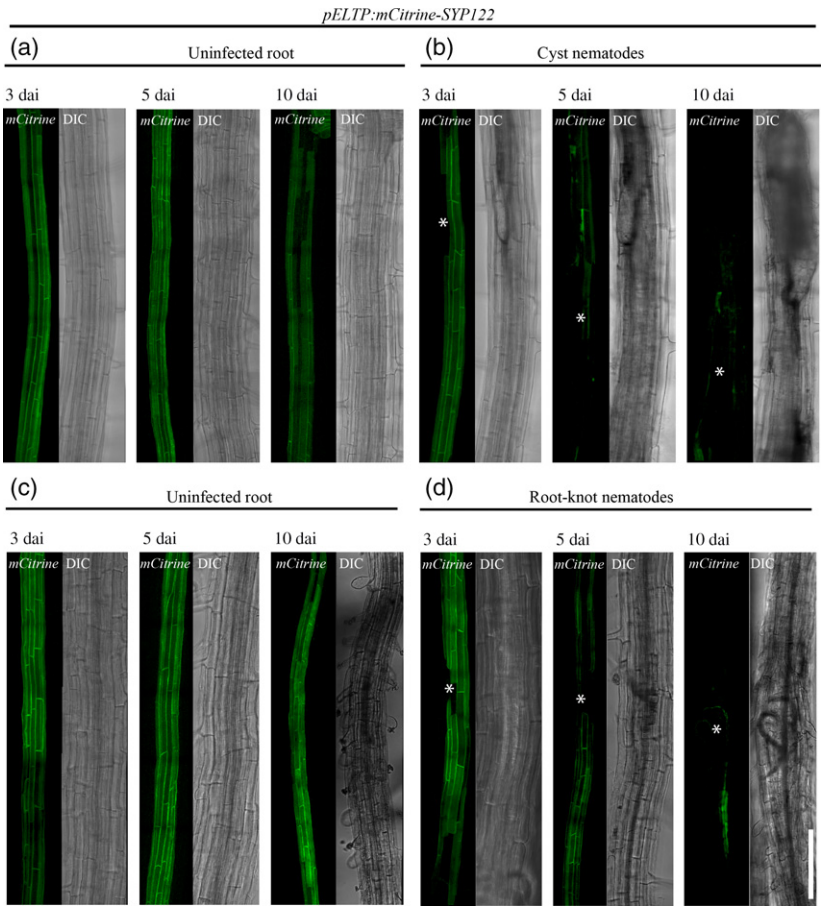

Figure 4. 3D Tile-scan (xyz) maximum projection images monitoring fluorescence signals of *pELTP:mCitrine-SYP122* upon infection. Here, 10–12-day old Arabidopsis plants were inoculated with second-stage juveniles (J2s) of cyst nematodes CN (a) or root-knot nematodes (RKN) (d) and images were taken at 3, 5 and 10 days after inoculation (dai). Asterisks indicate the nematode feeding site. Representative images are shown. Scale bar, 200 μm.

collected infection sites (Figure 5m,r) were less and smaller than around the syncytium (Figure 5n–q). These findings clearly indicate that CNs infection increases root development and formation of periderm (secondary cover tissue).

Although the endodermis was usually partly destroyed in roots infected with RKNs, it was still well recognizable around invaded J2s at 5 dai (Figure S3e). There was usually also no cell division in the pericycle in this region and at this time point. However, divisions of pericycle cells were fewer compared with 10 dai infection sites of CNs, and no recognizable endodermis was found in 10 dai samples of RKN infection sites (Figure S3f). Taken together, these observations supported our microscope data indicating degradation of the endodermis in nematode-infected regions around 5 dai. These data also explain differences observed in the expression of *pELTP:mCitrine-SYP122*, which is a marker for endodermis and showing that, in infected regions, degradation of the endodermis occurs earlier in CN infection sites than RKN sites.

Nematode infection sites are encircled by suberized tissue

To visualize suberin deposits, we employed a previously described protocol to stain infected and uninfected roots at 10 dai with the fluorescent dye Nile Red. Dissected galls and syncytia were cleared according to the ClearSee protocol (Kurihara *et al.*, 2015), stained and viewed under a confocal laser scanning microscope (Ursache *et al.*, 2018). We observed a specific red staining in non-infected control roots, as described previously (Figure 6). Upon infection, we found that the cell layer surrounding syncytia was stained specifically, indicating cohesive suberization of this tissue. In comparison with syncytia, staining of the cell layer surrounding the infection site induced by RKN appeared to be patchy (Figure 6).

Figure 5. Comparison of anatomy of infection sites containing syncytia induced by *Heterodera schachtii*. (a–f) Selected sections from single representative infection site with syncytium at 3 days after inoculation (dai); (g–l) selected sections from single representative infection site with syncytium at 5 dai; (m–r) selected sections from single representative infection site with syncytium at 10 dai. Parts (a), (g) and (m) (upper line) are directed towards the root base (basipetally), whereas parts (f), (l) and (r) (bottom line) are directed towards the root tip (acropetally). C, cortex; DC, detached/degraded cortex and epidermis; E, endodermis; Ep, epidermis; N, nematode; P, pericycle; Pd, periderm; S, syncytium; X, primary xylem. Asterisks indicate secondary xylem vessels. Scale bar: 20 μm. All figures were taken at the same magnification.

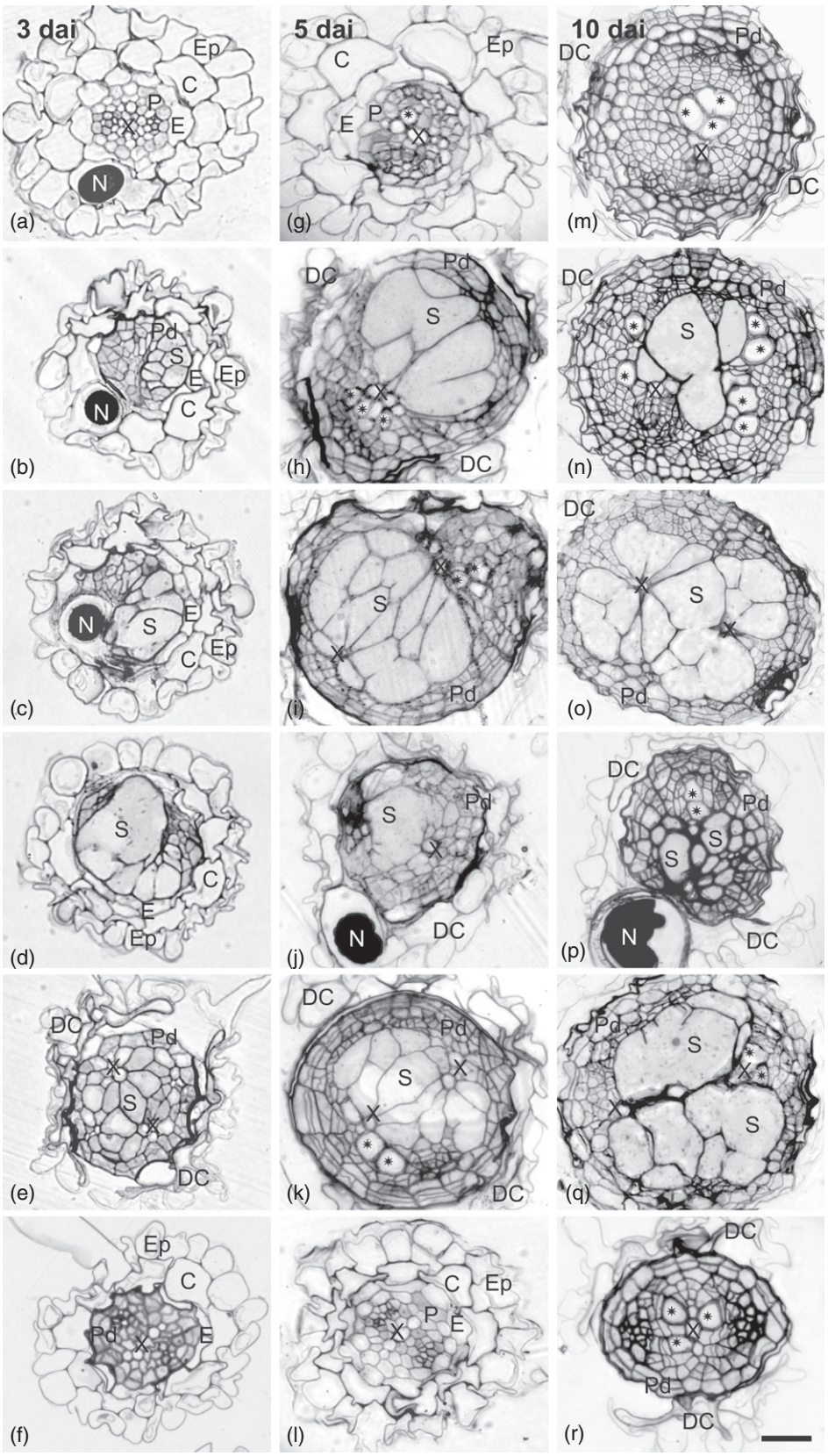

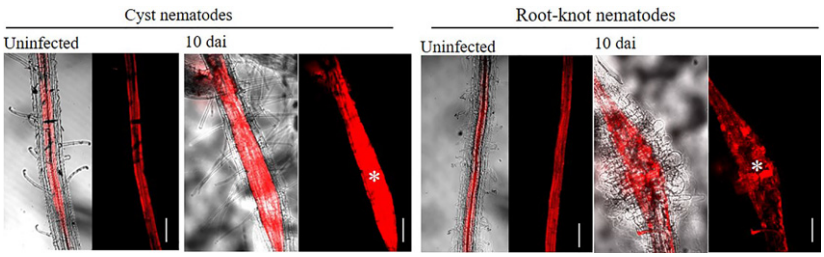

Figure 6. Fluorescence signal of Nile Red staining in infection sites induced by *Heterodera schachtii* and *Meloidogyne incognita*. Here, 10–12-day old Arabidopsis plants were inoculated with second-stage juveniles (J2s) and root segments containing infection sites were dissected at 10 days after inoculation (dai). Images are maximum intensity projections of Z-stacks. Asterisks represent nematode feeding site (syncytium or galls). Scale bar, 100 μm.

Suberin monomer composition is altered upon infection with nematodes

We next compared the chemical composition of aliphatic suberin in hand-sectioned root tissue containing syncytia and galls at 10 dai with that of uninfected control roots. There was no statistical difference in total aliphatic suberin content between nematode-infected root segments and control roots (Figure 7a). However, the abundance of single monomers was altered in nematode infection sites (Figure 7b,c). Levels of ω-hydroxyacids (ω-OH-acids) C18:1 and C16, α,ω-diacids C16 and C18, acid C20, and primary alcohol C18 were higher in aliphatic suberin extracted from *H. schachtii*-infected root segments than from control roots. Only the amounts of C24 primary fatty acid, alcohol, and α,ω-diacid were lower at these sites (Figure 7b). The monomer abundance in galls displayed a similar pattern; levels of ω-OH-acid C20, C18:1, and C16, α,ω-diacid C20, C18, and C16, primary alcohol C24, C20, and C18, and primary fatty acid C20 were higher than in control roots (Figure 7c).

Defective Casparian strips influence nematode infection and development

To characterize the role of the endodermis during plant–nematode interactions, we performed nematode infection assays with Arabidopsis lines altered in suberin deposits (*horst*, *pCASP1:CDEF1* (cuticle destructing factor 1)), CS formation (*sgn3-3*, *sgn3-3esb1-1*), or both (*esb1-1*, *esb1-1CDEF1*, *casp1-1casp3-1*) (Figure 8). The suberin mutant *horst* has 60% less aliphatic suberin than the wild-type and shows delayed suberin deposition (Höfer *et al.*, 2008; Naseer *et al.*, 2012), whereas *pCASP1:CDEF1* (expressing the suberin-degrading enzyme CDEF1 under the endodermis-specific CASP1 promoter (*pCASP1:CDEF1*)) lacks suberin throughout the root (Naseer *et al.*, 2012; Barberon *et al.*, 2016; Li *et al.*, 2017). The CS mutant s*gn3-3* is defective in CS formation, displaying a non-functional apoplastic barrier throughout the root system (Pfister *et al.*, 2014; Barberon *et al.*, 2016; Li *et al.*, 2017). In comparison, the mutant *esb1-1* only shows a delay in CS formation, which is compensated for by enhanced suberin deposition (ectopic suberin) starting close to the root tip, and accompanied by ectopic lignification in cell corners close to the CS. This abnormal suberization results in doubling of the amount of total aliphatic suberin compared with Col-0 (Baxter *et al.*, 2009; Hosmani *et al.*, 2013; Lee *et al.*, 2013; Li *et al.*, 2017). The double mutant *sgn3-3esb1-1* exhibited a more severe CS phenotype without ectopic suberization or lignification, due to the regulatory role of SGN3 in compensatory mechanisms (Pfister *et al.*, 2014). In *esb1-1CDEF1*, suberin was degraded by CDEF1 and ectopic lignification at the site of the CS, partially compensating for the lack of an apoplastic barrier. This compensatory mechanism, however, did not entirely seal the apoplast, which remained permeable, especially at lateral root emergence sites (Li *et al.*, 2017). A similar phenotype to *esb1-1* was displayed by the *casp1-1casp3-1* double mutant (Roppolo *et al.*, 2011; Hosmani *et al.*, 2013).

To perform nematode infection assays, plants were grown *in vitro* for 12 days and then infected with CN or RKN J2s. For CNs, we counted the number of females, and calculated their average size, and the average size of syncytia at 14 dai (Figure S4). For RKNs, we counted the number of galls and calculated their average area at 21 dai (Figure S5). From the suberin altered lines, *pCASP1:CDEF1* showed significant reduction of average syncytium size (Figure S4l). Similarly *casp1-1casp3-1* (defective CS/ectopic suberin and lignin) but not *esb1-1* showed a significantly reduced number of galls and smaller average female and syncytium sizes (Figures S4b,c and S5a). The most marked results were obtained in the CS-deficient lines *sgn3-3esb1-1*, and also in *esb1-1CDEF1* (CS defective/no ectopic suberin), which both affected infection by both nematode

Figure 7. Aliphatic suberin content in dissected root tissue containing syncytia (a, b) and galls (a, c). Here, 10–12-day old Arabidopsis plants were inoculated with *Heterodera schachtii* or *Meloidogyne incognita* second-stage juveniles (J2s) and root segments containing syncytia or galls were dissected at 10 days after inoculation (dai). Gas chromatography-mass spectrometry (GC-MS) analyses of total aliphatic suberin amounts and monomer composition were performed. Bars, means ± SD; ns, non-significant; *statistical significance relative to Col-0 wild-type (*t*-test, $P < 0.05$); $n = 3$. Plants were grown in Knop medium for *H. schachtii* infection assays and in Murashige and Skoog (MS) medium for root-knot nematode (RKN) infection assays.

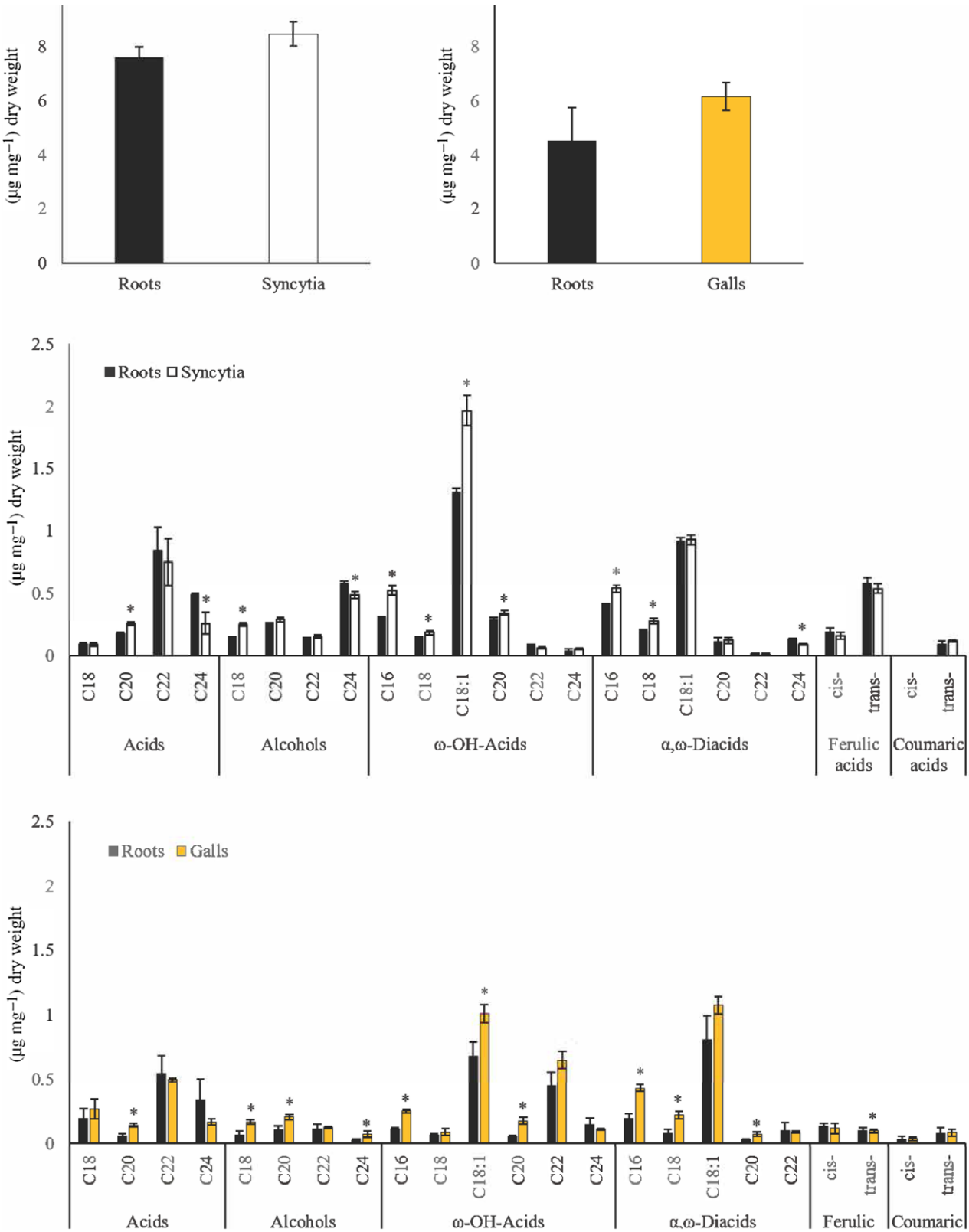

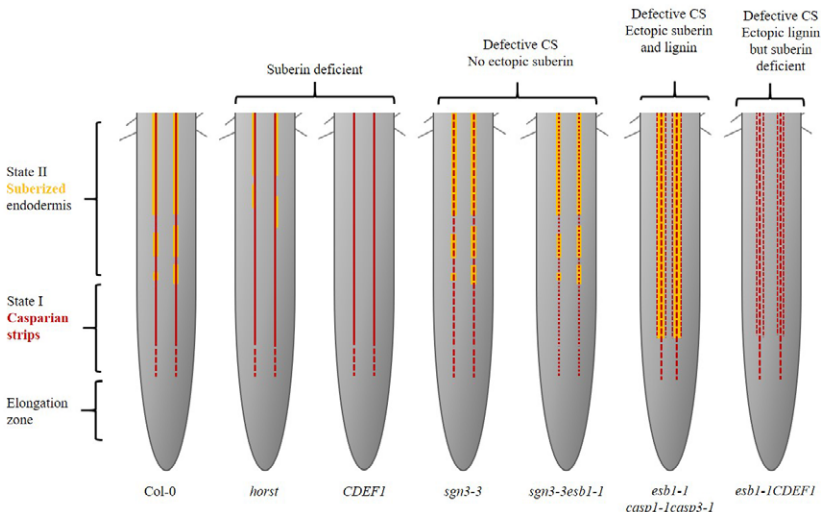

Figure 8. Schematic presentation of Casparian strips and suberin deposition in roots of different Arabidopsis phenotypes. In the wild-type Col-0 Casparian strip (CS) formation begins close to the root tip and is followed by suberization of the endodermis. The suberin deficient line *horst* shows reduced suberin deposition and *pCASP1:CDEF1* (*CDEF1*) lacks suberin completely. The CS deficient line *sgn3-3* shows defective CS formation, and *sgn3-3esb1-1* displays stronger defects in CS formation. The suberin and CS altered line *esb1-1* and *casp1-1-casp3-1* show defective CS accompanied by ectopic suberin and lignin deposition, whereas *esb1-1CDEF1* lacks suberin depositions but displays defective CS and ectopic lignin.

species (Figure 9). After CN infection, we observed a significant increase in the number of females and a significant increase in average syncytium size in *sgn3-3esb1-1* (defective CS/no ectopic suberin; Figure 9a,e). Similarly, we observed a significant decrease in the average female and syncytium size in *esb1-1CDEF1* (defective CS/suberin deficient but ectopic lignin) compared with Col-0 plants (Figure 9c,e). After RKN infection, we observed a significantly higher number of galls accompanied by a significantly lower average gall size in *sgn3-3esb1-1* and *esb1-1CDEF1* (Figure 9g) and a significantly reduced average gall size in *sgn3-3esb1-1*, *esb1-1CDEF1*, and *sgn3-3* (Figure 9i,j). Taken together, our data implied that a defective CS (without ectopic suberin) renders the plant more susceptible to nematode parasitism, particularly for *M. incognita*.

DISCUSSION

In the present study, we analyzed the role of suberin and CS, and the fate of endodermis in Arabidopsis roots during CN and RKN parasitism. We found that the expression of suberin biosynthesis genes was activated upon infection by both CN and RKN. In comparison with suberin biosynthesis genes, both CN and RKN infection showed only modest expression of the CS marker gene (*pCASP1:NLS3xmVenus*) during the early stages of infection (3 and 5 dai). Intriguingly, the expression of CS formation genes (*ESB1*, *SGN3*, *CASP1*) was downregulated or undetectable at 10 dai in both CN and RKN. This finding was supported by our microscope data and anatomical observations showed that feeding sites induced by both CN and RKN were surrounded by endodermis during early stages of infection. However, the endodermis was degraded during later stages of feeding site development, indicating periderm formation. Based on our observations, we proposed that nematode infection causes damage to the endodermis and induced periderm development that consequently activated suberin biosynthesis genes at the site of infection. However, once a feeding site was established and expanded, increased expression of suberin biosynthesis genes was only required at highly localized patches where phellogen cells differentiate into phellem cells that had suberized cell walls.

We found that the tissue surrounding syncytia and galls underwent *de novo* suberization. Although the detected suberin monomers were characteristic of Arabidopsis roots (Franke *et al.*, 2005), we found a consistent change in suberin composition in nematode infection sites. This change in monomer composition and anatomical observations supported our hypothesis that nematode infection induces periderm formation that encompass *de novo* suberization of phellem cells at the site of infection. Notably, the change in suberin monomer composition was supported by upregulation of several genes involved in their biosynthesis. For example, we detected an increase in C18:1 and C16 ω-OH-acids in root segments containing syncytia at 10 dai. Additionally, ω-OH-acids, which are precursors of α, ω-dicarboxylic acids, and the corresponding C16 and C18 chain lengths, were significantly increased. Changes in these

Figure 9. Nematode infection assays. *sgn3-3*, *sgn3-3esb1-1* (defective Casparian strip (CS)), and *esb1-1CDEF1* (defective CS/suberin deficient) were inoculated with *Heterodera schachtii* (a–f) or *Meloidogyne incognita* (g–j). Here, 10–12-day old Arabidopsis plants were inoculated with second-stage juveniles (J2s). At 13 days after inoculation (dai) number of females was counted and at 14 dai images of females and syncytia or galls were taken to measure the sizes in mm^2. Rep. (repetition), independent experiments; bars, means ± SE; Data were analyzed using single-factor analysis of variance (ANOVA) and Tukey's post hoc test. Values not sharing same letter are significantly different from each other ($P < 0.05$); $n = 40–60$.

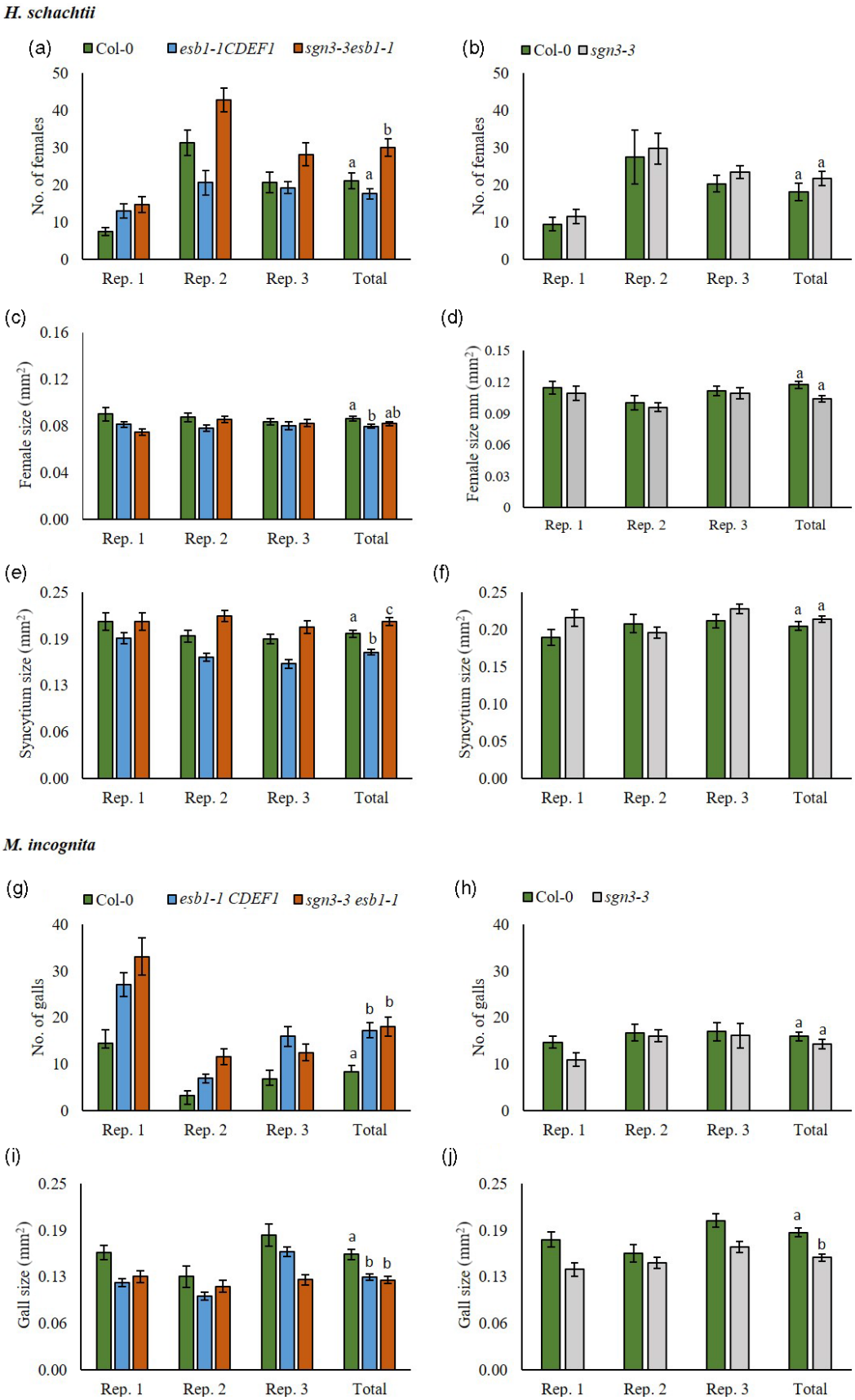

monomers have previously been shown to be associated with the expression of *CYP86A1* (Höfer *et al.*, 2008) and we also observed a significant increase in *CYP86A1* expression upon CN infection. Similarly, we found significant increase in C20 precursors that is likely to be related to activation of *GPAT5* upon CN infection. The increase in levels in the primary alcohol C18 might be due to upregulation of *FAR4*. However, there was no significant increase in C20 primary alcohol levels, despite an increase in *FAR4* transcript levels (Domergue *et al.*, 2010). Recently it has been shown that most esterified fatty alcohols are a major compound of suberin-associated waxes (Delude *et al.*, 2016). Although, the suberin extraction method used here did not allow detection of associated waxes, upregulation of *FAR5* indicated that the level of C20 primary alcohol could be increased in the associated waxes. In contrast, galls showed a significant increase in C20 primary alcohol levels at 10 dai. Overall, especially the patterns of ω-OH-acids and primary fatty acids showed similarities to peridermal suberin as found in roots undergoing secondary development (Höfer *et al.*, 2008) and supported our anatomical observations that development of nematode feeding site induced and enhanced the formation of the secondary state of growth (including formation of periderm) in infected root regions. Our measurements of nematode-infected tissue showed similar suberin monomer abundances between syncytia and galls, which were significantly different from uninfected root tissue.

Our expression data, microscopy observations, and biochemical measurements established that both CN and RKN infection induced a characteristic suberization pattern at the infection site, and indicated that suberin has an important role during nematode parasitism. However, alterations in endodermal suberin did not result in significant changes in infection assays. It is possible that reduced suberin levels cause subtle changes in aspects of parasitism (such as feeding site initiation, nutrient availability, parasite maturation, and reproductive success), which might not lead to significant effects in the parameters used in this study. In contrast, nematode infection assays showed that lines with defects in 'CS formation without ectopic suberin' had significantly increase in the numbers of both CNs (*sgn3-3esb1-1*) and RKNs (*sgn3-3esb1-1* and *esb1-1CDEF1*) and significantly decreased average sizes of females (*esb1-1CDEF1*), syncytia (*esb1-1CDEF1*), and galls (*sgn3-3*, *sgn3-3esb1-1* and *esb1-1CDEF1*) compared with the control. In addition to having defective CS formation, *sgn3-3*, *sgn3-3esb1-1*, and *esb1-1CDEF1* were also impaired in the compensatory suberization mechanism sealing CS defects, as these mutants are unable to deposit ectopic suberin. It has been previously shown that non-functional SGN3 in *sgn3-3* and *sgn3-3esb1-1* led to a breakdown of the compensatory barrier surveillance system (Doblas *et al.*, 2017b; Nakayama *et al.*, 2017). A similar effect was achieved by CDEF1 in *esb1-1CDEF1*, which degrades newly formed suberin (Naseer *et al.*, 2012). Therefore, holes in the CS barrier were not sealed by suberin in these mutants. Intriguingly, *esb1-1CDEF1* showed ectopic lignification close to the corner of the cells, which can be seen as a reinforced apoplastic barrier line. Nevertheless, the inability of ectopic lignin to seal newly formed holes in the endodermis has been observed in *esb1-1CDEF1* at lateral root emergence sites, which were the only entry points for the apoplastic tracer propidium iodide (Li *et al.*, 2017). These holes in the apoplastic barrier might make it easier for nematodes to reach the vascular cylinder and establish their feeding site. Intriguingly, we found that CS defects had a much more pronounced effect on RKNs than on CNs, unravelling what may be a key difference in migration habit between the two nematode species. CNs move intracellularly and are able to cross the endodermis directly, whereas RKNs move intercellularly and circumvent the CS by migrating to the meristematic region and then making a U-turn to enter the vasculature (Sijmons *et al.*, 1991; Wyss *et al.*, 1992). Therefore, unsealed holes in the endodermis might provide additional entry points into the vasculature, contributing to the higher infectivity of RKNs.

However, our infection assays also revealed reduced average feeding site sizes (*sgn3-3*, *sgn3-3esb1-1*, and *esb1-1CDEF1*), indicating a role for the endodermis during nematode nutrient acquisition. The expression pattern of *pCASP1:NLS3xmVenus* in the early biotrophic stages of nematode parasitism indicated that CS formation remains functional in infection sites and that CS may play a role in nutrient homeostasis for nematodes. The CS seals the apoplast and plays a vital role in plant nutrient homeostasis by preventing diffusion out of the central vasculature. A discontinuous CS increased the permeability of solutes, therefore impairing nutrient availability. These effects on nutrient status have been previously described in detail for several suberin- and CS-affected lines (reviewed in Barberon, 2017; Doblas *et al.*, 2017a). Giant cells and syncytia act as metabolic sinks and share features of nutrient transfer cells. Both types of feeding sites are surrounded by a dense network of xylem vessels and phloem sieve tubes, which are formed *de novo*. Although similarities have been drawn between the function of syncytia and galls, there are fundamental differences in how nutrients are transported towards and into these two different feeding sites (Jones and Northcote, 1972; Hoth *et al.*, 2008; Siddique and Grundler, 2015). Young syncytia are symplasmically isolated and nutrients are supplied by active transport (Hofmann and Grundler, 2006; Hofmann *et al.*, 2007). During syncytium development, secondary phloem elements are formed and plasmodesmata enable symplasmic transport from sieve elements into syncytium (Hoth *et al.*, 2005; Hofmann *et al.*, 2007; Absmanner *et al.*, 2013). Therefore, nutrient uptake into syncytia changes from active to

symplasmic transport during nematode development (Hofmann *et al.*, 2007; Hoth *et al.*, 2008). In comparison with syncytia, giant cells remain symplasmically isolated throughout their life cycle and newly formed secondary phloem sieve tubes that lack companion cells surround the giant cells (Hoth *et al.*, 2008; Absmanner *et al.*, 2013). In galls, solutes are unloaded from sieve elements into the apoplast from which the nutrients are further transported into the symplasmically isolated giant cells (Bartlem *et al.*, 2013). Hence, in galls, nutrients temporarily reside in the apoplastic space between sieve elements and giant cells. Normally, the loss of these nutrients into surrounding tissue or the soil is prevented by the CS barrier. Therefore, defects in CS formation, not compensated for by suberization, would lead to an outflow of solutes, which may impair nematode development.

Based on these data, we proposed that nematode feeding site development ruptures the apoplastic seal of the endodermis, and triggers a compensatory suberin mechanism induced by the barrier surveillance system (Doblas *et al.*, 2017b; Nakayama *et al.*, 2017). When this programme is inoperable and the ability of the endodermis to seal itself is impaired, and nutrients leak out of the vasculature, leading to deficiencies for both the plant and the parasite. A consequence of this reduced nutrient state is reduced growth rates, reflected in the reduced size of the feeding sites.

CONCLUSION

Our results imply that a functional endodermis constitutes a hurdle to nematode penetration and can therefore be considered as part of preformed defences. The endodermal tissue is maintained around the nematode feeding site during early stages of infection and *M. incognita* especially benefits from this for infection and nutrient acquisition. Taken together, the endodermis plays a dual role in nematode parasitism, a barrier to nematode entrance and a regulator of nutrient acquisition for nematodes from feeding sites. The overall modest impact of the CS and suberin alterations on nematode infection possibly underlies compensatory mechanisms such as the upregulation of influx carriers (Pfister *et al.*, 2014; Barberon *et al.*, 2016). Changes in suberin monomer composition are most likely to be triggered by the sensitive barrier surveillance system in the endodermis that maintains its sealing properties despite infestation by nematodes (Doblas *et al.*, 2017b; Nakayama *et al.*, 2017).

EXPERIMENTAL PROCEDURES

Plant material and growth conditions

Arabidopsis thaliana ecotype Columbia (Col-0) was used for all experiments. Plants were grown in Petri dishes containing agar medium. *H. schachtii* infection assays were performed on 0.8% (w/v) Daichin (Duchefa Biochemie) agar medium enriched with modified Knop nutrient solutions as described previously (Sijmons *et al.*, 1991) with 2% (w/v) sucrose and 0.1% (w/v) 100× Gamborg's vitamin solution (Sigma-Aldrich). Infection assays with *M. incognita* were conducted in Murashige and Skoog medium including vitamin and MES buffer (Duchefa Biochemie) supplemented with 0.5% (w/v) Gelrite (Roth) and 2% (w/v) sucrose. Seeds were surface sterilized and plants were grown under conditions described previously (Hütten *et al.*, 2015). The following T-DNA insertion lines were used for infection assays: *horst-1* (*cyp86a1*, AT5G58860) (Höfer *et al.*, 2008), *sgn3-3* (AT4G20140) (Pfister *et al.*, 2014), the leaf ionomic line *esb1-1* (AT2G28670) (Baxter *et al.*, 2009), the double mutants *sgn3-3esb1-1* (Pfister *et al.*, 2014) and *casp1-1casp3-1* (AT2G36100/AT2G27370) (Roppolo *et al.*, 2011), and lines *pCASP1:CDEF1* (Naseer *et al.*, 2012) and *esb1-1CDEF1* (Li *et al.*, 2017), containing the suberin-degrading enzyme CDEF1 expressed under the endodermis-specific CASP1 promoter. *pGPAT5:mCitrine-SYP122* was crossed into the *sgn3-3* background.

Nematode cultures and inoculum

Heterodera schachtii was propagated and second-stage juveniles (J2) were hatched as described previously (Siddique *et al.*, 2009). Freshly hatched J2 were surface sterilized with 0.05% (w/v) mercury chloride. Here, 60–80 J2s in a water suspension were inoculated onto the agar surface above the root system of 10- to 12-day-old plants. Petri dishes were stored under standard growth conditions, as described above.

Meloidogyne incognita was propagated and eggs were extracted as described previously (Mendy *et al.*, 2017). To separate freshly extracted eggs from soil particles, the eggs were suspended in a 35% (w/v) sucrose solution and centrifuged. Eggs and freshly hatched J2s were surface sterilized as described previously (Mendy *et al.*, 2017). The roots of 10- to 12-day-old plants were inoculated with 90–100 sterile J2s and the plants were stored under standard growth conditions in darkness (see above).

Infection assays and measurements

For each experiment, 10–20 plants were used per genotype, and experiments were repeated three times independently. For *H. schachtii* infection assays, the number of female nematodes was counted at 14 dai and females and syncytia were photographed. For *M. incognita* infection, the number of galls was counted at 21 dai and galls were photographed. Photographs were used for the area measurements of galls, syncytia, and *H. schachtii* females using Leica Application Suite software. In total, 90–150 individual infection sites were photographed for each genotype with a Leica M165C, Camera Leica DFC450C (Leica Microsystems, Wetzlar, Germany).

GUS staining procedure

The activity of previously described promoter:GUS fusions *pCYP86A1:GUS* (Höfer *et al.*, 2008) was analyzed by GUS staining. A 5-bromo-4-chloro-3-indolyl-β-D-glucuronide (1 mM X-Gluc) solution was poured onto the agar surface in Petri dishes and incubated at 38°C as described in Siddique *et al.* (2009). The *pCYP86A1:GUS* line was incubated overnight. Photographs were taken using a Leica DMI 4000B camera DFC450C (Leica Microsystems).

Fluorescence microscopy

The transcriptional reporter lines *pCASP1:NLS3xmVenus* (AT2G36100) (Vermeer *et al.*, 2014; Barberon *et al.*, 2016) and

pGPAT5:mCitrine-SYP122 (AT3G11430) (Barberon *et al.*, 2016) were examined using a Zeiss LSM 710 (Zeiss, Oberkochen, Germany) confocal laser scanning microscope. Plants were grown on coverslips (24 × 60 mm) covered with 3 mL agar medium. Pictures were taken with a ×40 water immersion objective. Maximum intensity projections of confocal Z-stacks were obtained using ImageJ software (NIH; http://rsb.info.nih.gov/ij) and Zeiss Zen2.1 (black edition) software.

A Zeiss LSM 880 inverted confocal scanning microscope was used for Tile scanning, Pictures were taken with a ×40 water immersion objective. For more detailed analyses, imaging was performed with Z-scans plus Tile-scans (overlap 20%). Fluorescence signals for *mCitrine* (excitation 514 nm, emission 515–550 nm), was detected. Images were analyzed and processed/edited using ImageJ (NIH; http://rsb.info.nih.gov/ij) and Zeiss Zen2.1 (black edition) software.

Reverse-transcription quantitative PCR (qPCR)

Infection sites induced by *H. schachtii* and *M. incognita* on Col-0 plants were hand-dissected at 10 dai and immediately frozen in liquid nitrogen. Three biological replicates were collected, each containing ~100 mg fresh root weight, which included ≥300 feeding sites (per replicate). Uninfected roots, excluding root tips, served as controls. Total RNA was extracted using the RNeasy Plant Mini Kit (Qiagen, Hilden, Germany) according to the manufacturer's instructions. RNA samples were treated with DNA-free DNase Treatment & Removal (Ambion, Life Technologies, Darmstadt, Germany) and the quality was tested using a 2100 Bioanalyzer (Agilent Technologies, Heidelberg, Germany) on an RNA NanoChip. The isolated RNA was transcribed into cDNA using random primers and the High Capacity cDNA Reverse-Transcription Kit (Applied Biosystems, Darmstadt, Germany). The samples were analyzed with the StepOne Plus Real-Time PCR System (Applied Biosystems) in 20 μl reactions containing 10 μl Fast SYBR Green qPCR Master Mix, 0.75 μl forward and reverse primer (10 μM) each, 1 μl cDNA, and sterile RNase/DNase free water. For internal references, β-tubulin 4 and 18S rRNA were used with a 1:100 dilution of cDNA. qPCR was carried out as described previously (Hütten *et al.*, 2015). Relative expression was calculated according to Pfaffl (2001). Primers are listed in Table S2.

Anatomy of infected roots

A. thaliana Col-0 plants were grown and inoculated with J2s of *H. schachtii* or *M. incognita* as described above. Root segments (*c.* 5 mm long) containing feeding sites at 3, 5 and 10 dai were dissected and processed for microscopic examinations as described by Golinowski *et al.* (1996) and Sobczak *et al.* (1997). Semi-thin sections were stained with hot 0.1% (w/v) toluidine blue (pH 6.8) and examined under an Olympus AX70 'Provis' (Olympus, Tokyo, Japan) light microscope equipped with an Olympus UC90 digital camera (Olympus). Ultra-thin sections were examined under an FEI 268D 'Morgagni' (ThermoFisher Scientific, Waltham, MA, USA) transmission electron microscope operating at 80 kV. Images were taken with an Olympus-SIS 'Morada' digital camera. Images were processed for similar contrast and brightness using Adobe Photoshop (Adobe Corp., San Jose, CA, USA) software.

Histochemical suberin staining

Dissected infection sites (10 dai) were fixed in 4% (w/v) paraformaldehyde in 1× PBS buffer for 1 h at RT and washed twice for 1 min in PBS buffer. Fixed root samples were incubated for 10 days at RT in ClearSee solution in dark (Kurihara *et al.*, 2015). Cleared root sections were incubated overnight in fresh ClearSee solution containing 0.05% Nile Red (Sigma, CAS-No: 7385-67-3) and examined using a Zeiss LSM 710 (Ursache *et al.*, 2018). Maximum intensity projections of confocal Z-stacks were obtained using ImageJ software (version 1.48v, National Institutes of Health, USA, http://imagej.nih.gov/ij).

Suberin analyses

For aliphatic suberin monomer extraction, three technical replicates of dissected infection sites (10 dai) from ≥30 plants (~450–600 mg fresh weight) and control roots of uninfected plants were frozen in liquid nitrogen. To remove unbound lipids, samples were extracted for 24 h in methanol and chloroform, dried, and weighed. Samples were depolymerized and injected on-column on an Agilent 6890N gas chromatograph (GC) combined with an Agilent 5973N quadrupole mass-selective detector for monomer identification and for quantitative analysis based on an internal standard using an identical GC system coupled with a flame ionization detector, as described previously (Franke *et al.*, 2005).

ACKNOWLEDGEMENTS

We appreciate the excellent technical assistance of Stefan Neumann, Gisela Sichtermann, and Thomas Gerhardt and are thankful for the dedication of Andre Krause, Tilmann Brunnberg, Chanz Robbins, and Phyo Wai Htike. We acknowledge Michael Hoch for providing access to the confocal microscope and to Bernhard Fuß for technical assistance. We are very thankful to Casper van Schaik and Aska Goverse for sharing the protocol on root-knot nematode sterilization. Finally, we thank David Salt and Marie Barberon for kindly providing seeds. This work was supported by the *Deutsche Forschungsgemeinschaft* (DFG) within the framework of the 1st call ERA-NET for Coordinating Plant Sciences (ERA-CAPS) (grant GR1161/10-1 to FMWG and FR1721/2-1 to RBF) and by the Federation of European Biochemical Sciences Postdoctoral Long-Term Fellowship to PM.

CONFLICT OF INTERESTS

The authors declare there is no conflict of interest.

AUTHOR CONTRIBUTIONS

SS conceptualized the study and designed the experiments with input from JH, FMWG, LS, RBF, MS and NG. JH performed the majority of the experiments. PM performed the confocal microscopy experiments with help from SF. MS and MG performed anatomical observations. JH curated the data and performed the statistics. SS and JH wrote the manuscript with input from all authors.

DATA STATEMENT

All data referred to are included in the manuscript or supplementary materials of this manuscript.

SUPPORTING INFORMATION

Additional Supporting Information may be found in the online version of this article.

Table S1. Expression of suberin- and Casparian strip (CS)-related genes in *Meloidogyne incognita* (GC and Gall) and *Heterodera schachtii* (Sync) infection sites.

Table S2. Primer list for qPCR.

Figure S1. Activity of *pCYP86A: GUS* in infection sites induced by *Heterodera schachtii* (a) and *Meloidogyne incognita* (b) at 3, 5 and 10 days after inoculation (dai).

Figure S2. Fluorescence signals of *pCASP1:NLS3xmVenus* in infection sites.

Figure S3. Ultrastructure and anatomy of uninfected and nematode-infected roots.

Figure S4. Results of *Heterodera schachtii* infection assays in Casparian strip (CS) and suberin mutants.

Figure S5. Results of *Meloidogyne incognita* infection assays in Casparian strip (CS) and suberin mutants.

REFERENCES

Absmanner, B., Stadler, R. and Hammes, U.Z. (2013) Phloem development in nematode-induced feeding sites: the implications of auxin and cytokinin. *Front. Plant Sci.* **4**, 241.

Alassimone, J., Fujita, S., Doblas, V.G. *et al.* (2016) Polarly localized kinase SGN1 is required for Casparian strip integrity and positioning. *Nat. Plants*, **2**, 16113.

Balhadère, P. and Evans, A. (1995) Cytochemical investigation of resistance to root-knot nematode *Meloidogyne naasi* in cereals and grasses using cryosections of roots. *Fundam. Appl. Nematol.* **18**, 539–547.

Barberon, M. (2017) The endodermis as a checkpoint for nutrients. *New Phytol.* **213**, 1604–1610.

Barberon, M., Vermeer, J.E.M., De Bellis, D. *et al.* (2016) Adaptation of root function by nutrient-induced plasticity of endodermal differentiation. *Cell*, **164**, 447–459.

Barcala, M., García, A., Cabrera, J., Casson, S., Lindsey, K., Favery, B., García-Casado, G., Solano, R., Fenoll, C. and Escobar, C. (2010) Early transcriptomic events in microdissected Arabidopsis nematode-induced giant cells. *Plant J.* **61**, 698–712.

Bartlem, D.G., Jones, M.G.K. and Hammes, U.Z. (2013) Vascularization and nutrient delivery at root-knot nematode feeding sites in host roots. *J. Exp. Bot.* **65**, 1789–1798.

Baxter, I., Hosmani, P.S., Rus, A., Lahner, B., Borevitz, J.O., Muthukumar, B., Mickelbart, M.V., Schreiber, L., Franke, R.B. and Salt, D.E. (2009) Root suberin forms an extracellular barrier that affects water relations and mineral nutrition in Arabidopsis. *PLoS Genet.* **5**, e1000492.

Beisson, F., Li, Y., Bonaventure, G., Pollard, M. and Ohlrogge, J.B. (2007) The acyltransferase GPAT5 is required for the synthesis of suberin in seed coat and root of Arabidopsis. *Plant Cell*, **19**, 351–368.

Cabrera, J., Bustos, R., Favery, B., Fenoll, C. and Escobar, C. (2014) NEMATIC: a simple and versatile tool for the in silico analysis of plant-nematode interactions. *Mol. Plant Pathol.* **15**, 627–636.

Compagnon, V., Diehl, P., Benveniste, I., Meyer, D., Schaller, H., Schreiber, L., Franke, R. and Pinot, F. (2009) CYP86B1 is required for very long chain omega-hydroxyacid and alpha, omega -dicarboxylic acid synthesis in root and seed suberin polyester. *Plant Physiol.* **150**, 1831–1843.

Delude, C., Fouillen, L., Bhar, P., Cardinal, M.J., Pascal, S., Santos, P., Kosma, D.K., Joubès, J., Rowland, O. and Domergue, F. (2016) Primary fatty alcohols are major components of suberized root tissues of Arabidopsis in the form of alkyl hydroxycinnamates. *Plant Physiol.* **171**, 1934–1950.

Doblas, V.G., Geldner, N. and Barberon, M. (2017a) The endodermis, a tightly controlled barrier for nutrients. *Curr. Opin. Plant Biol.* **39**, 136–143.

Doblas, V.G., Smakowska-Luzan, E., Fujita, S., Alassimone, J., Barberon, M., Madalinski, M., Belkhadir, Y. and Geldner, N. (2017b) Root diffusion barrier control by a vasculature-derived peptide binding to the SGN3 receptor. *Science*, **355**, 280–284.

Dolan, L. and Roberts, K. (1995) Secondary thickening in roots of *Arabidopsis thaliana*: anatomy and cell surface changes. *New Phytol.* **131**, 121–128.

Domergue, F., Vishwanath, S.J., Joubès, J. *et al.* (2010) Three Arabidopsis fatty acyl-coenzyme A reductases, FAR1, FAR4, and FAR5, generate primary fatty alcohols associated with suberin deposition. *Plant Physiol.* **153**, 1539–1554.

Franke, R., Briesen, I., Wojciechowski, T., Faust, A., Yephremov, A., Nawrath, C. and Schreiber, L. (2005) Apoplastic polyesters in Arabidopsis surface tissues–A typical suberin and a particular cutin. *Phytochemistry*, **66**, 2643–2658.

Franke, R.B., Höfer, R., Briesen, I., Emsermann, M., Efremova, N., Yephremov, A. and Schreiber, L. (2009) The DAISY gene from Arabidopsis encodes a fatty acid elongase condensing enzyme involved in the biosynthesis of aliphatic suberin in roots and the chalaza-micropyle region of seeds. *Plant J.* **57**, 80–95.

Golinowski, W., Grundler, F.M.W. and Sobczak, M. (1996) Changes in the structure of Arabidopsis thaliana during female development of the plant-parasitic nematode *Heterodera schachtii*. *Protoplasma*, **194**, 103–116.

Gou, J.-Y., Yu, X.-H. and Liu, C.-J. (2009) A hydroxycinnamoyltransferase responsible for synthesizing suberin aromatics in Arabidopsis. *Proc. Natl Acad. Sci. USA*, **106**, 18855–18860.

Höfer, R., Briesen, I., Beck, M., Pinot, F., Schreiber, L. and Franke, R. (2008) The Arabidopsis cytochrome P450 CYP86A1 encodes a fatty acid omega-hydroxylase involved in suberin monomer biosynthesis. *J. Exp. Bot.* **59**, 2347–2360.

Hofmann, J. and Grundler, F.M.W. (2006) Females and males of root-parasitic cyst nematodes induce different symplasmic connections between their syncytial feeding cells and the phloem in *Arabidopsis thaliana*. *Plant Physiol. Biochem.* **44**, 430–433.

Hofmann, J., Wieczorek, K., Blöchl, A. and Grundler, F.M.W. (2007) Sucrose supply to nematode-induced syncytia depends on the apoplasmic and symplasmic pathways. *J. Exp. Bot.* **58**, 1591–1601.

Holbein, J., Grundler, F.M.W. and Siddique, S. (2016) Plant basal resistance to nematodes: an update. *J. Exp. Bot.* **67**, 2049–2061.

Hosmani, P.S., Kamiya, T., Danku, J., Naseer, S., Geldner, N., Lou, Guerinot M. and Salt, D.E. (2013) Dirigent domain-containing protein is part of the machinery required for formation of the lignin-based Casparian strip in the root. *Proc. Natl Acad. Sci. USA*, **110**, 14498–14503.

Hoth, S., Schneidereit, A., Lauterbach, C., Scholz-Starke, J. and Sauer, N. (2005) Nematode infection triggers the de novo formation of unloading phloem that allows macromolecular trafficking of green fluorescent protein into syncytia. *Plant Physiol.* **138**, 383–392.

Hoth, S., Stadler, R., Sauer, N. and Hammes, U.Z. (2008) Differential vascularization of nematode-induced feeding sites. *Proc. Natl Acad. Sci. USA*, **105**, 12617–12622.

Hütten, M., Geukes, M., Misas-Villamil, J.C., van der Hoorn, R.A.L., Grundler, F.M.W. and Siddique, S. (2015) Activity profiling reveals changes in the diversity and activity of proteins in Arabidopsis roots in response to nematode infection. *Plant Physiol. Biochem.* **97**, 36–43.

Jones, M.G.K. and Northcote, D.H. (1972) Nematode-induced syncytium—a multinucleate transfer cell. *J. Cell Sci.* **10**, 789–809.

Juvale, P.S. and Baum, T.J. (2018) 'Cyst-ained' research into Heterodera parasitism. *PLoS Pathog.* **14**, e1006791.

Kurihara, D., Mizuta, Y., Sato, Y. and Higashiyama, T. (2015) ClearSee: a rapid optical clearing reagent for whole-plant fluorescence imaging. *Development*, **142**, 4168–4179.

Kyndt, T., Vieira, P., Gheysen, G. and de Almeida-Engler, J. (2013) Nematode feeding sites: unique organs in plant roots. *Planta*, **238**, 807–818.

Lee, Y., Rubio, M.C., Alassimone, J. and Geldner, N. (2013) A mechanism for localized lignin deposition in the endodermis. *Cell*, **153**, 402–412.

Li, B., Kamiya, T., Kalmbach, L. *et al.* (2017) Role of LOTR1 in nutrient transport through organization of spatial distribution of root endodermal barriers. *Curr. Biol.* **27**, 758–765.

Marhavý, P., Kurenda, A., Siddique, S., Tendon, D.V., Zhou, F., Holbein, J., Shahim, H.M., Grundler, F.M.W., Farmer, E.E. and Geldner, N. (2019) Single cell damage elicits regional, nematode-restricting ethylene responses in roots. *EMBO J.* **38**, e100972.

Mendy, B., Wang'ombe, M.W., Radakovic, Z.S., Holbein, J., Ilyas, M., Chopra, D., Holton, N., Zipfel, C., Grundler, F.M., Siddique, S. (2017) Arabidopsis leucine-rich repeat receptor–like kinase NILR1 is required for induction of innate immunity to parasitic nematodes. *PLoS Pathog.* **13**, e1006284.

Molina, I., Li-Beisson, Y., Beisson, F., Ohlrogge, J.B. and Pollard, M. (2009) Identification of an Arabidopsis feruloyl-coenzyme A transferase required for suberin synthesis. *Plant Physiol.* **151**, 1317–1328.

Nakayama, T., Shinohara, H., Tanaka, M., Baba, K., Ogawa-Ohnishi, M. and Matsubayashi, Y. (2017) A peptide hormone required for Casparian strip diffusion barrier formation in Arabidopsis roots. *Science*, **355**, 284–286.

Naseer, S., Lee, Y., Lapierre, C., Franke, R., Nawrath, C. and Geldner, N. (2012) Casparian strip diffusion barrier in Arabidopsis is made of a lignin polymer without suberin. *Proc. Natl Acad. Sci. USA*, **109**, 10101–10106.

Nicol, J.M., Turner, S.J., Coyne, D.L., den Nijs, L., Hockland, S. and Tahna Maafi, Z. (2011) Current nematode threats to world agriculture. In *Genomics and Molecular Genetics of Plant-Nematode Interactions*. (Jones, J., Gheysen, G. and Fenoll, C., eds). Dorderecht: Springer, pp. 21–44.

Pfaffl, M.W. (2001) A new mathematical model for relative quantification in real-time RT-PCR. *Nucleic Acids Res.* **29**, e45.

Pfister, A., Barberon, M., Alassimone, J. *et al.* (2014) A receptor-like kinase mutant with absent endodermal diffusion barrier displays selective nutrient homeostasis defects. *eLife*, **3**, e03115.

Radakovic, Z.S., Anjam, M.S., Escobar, E., Chopra, D., Cabrera, J., Silva, A.C., Escobar, C., Sobczak, M., Grundler, F.M.W. and Siddique, S. (2018) Arabidopsis *HIPP27* is a host susceptibility gene for the beet cyst nematode *Heterodera schachtii*. *Mol. Plant Pathol.* **19**, 1917–1928.

Roppolo, D., De Rybel, B., Tendon, V.D., Pfister, A., Alassimone, J., Vermeer, J.E.M., Yamazaki, M., Stierhof, Y.-D., Beeckman, T. and Geldner, N. (2011) A novel protein family mediates Casparian strip formation in the endodermis. *Nature*, **473**, 380–383.

Różańska, E., Czarnocka, W., Baranowski, Ł., Mielecki, J., de Almeida, Engler J. and Sobczak, M. (2018) Expression of both *Arabidopsis* γ-tubulin genes is essential for development of a functional syncytium induced by *Heterodera schachtii*. *Plant Cell Rep.* **37**, 1279–1292.

Shah, S.J., Anjam, M.S., Mendy, B., Anwer, M.A., Habash, S.S., Lozano-Torres, J.L., Grundler, F.M.W. and Siddique, S. (2017) Damage-associated responses of the host contribute to defence against cyst nematodes but not root-knot nematodes. *J. Exp. Bot.* **68**, 5949–5960.

Siddique, S., Grundler, F.M.W. (2015). Metabolism in nematode feeding sites. In *Plant Nematode Interactions: A View on Compatible Interrelationships* (Escobar, C. and Fenoll, C., eds). New york, NY: Elsevier Ltd, pp. 119–138.

Siddique, S. and Grundler, F.M.W. (2018) Parasitic nematodes manipulate plant development to establish feeding sites. *Curr. Opin. Microbiol.* **46**, 102–108.

Siddique, S., Endres, S., Atkins, J.M. ***et al.*** (2009) Myo-inositol oxygenase genes are involved in the development of syncytia induced by *Heterodera schachtii* in Arabidopsis roots. *New Phytol.* **184**, 457–472.

Siddique, S., Radakovic, Z.S., Carola, M. ***et al.*** (2015) A parasitic nematode releases cytokinin that controls cell division and orchestrates feeding site formation in host plants. *Proceedings of the National Academy of Sciences*, **112**(41), 12669–12674.

Sijmons, P., Grundler, F., von Mende, N., Burrows, P. and Wyss, U. (1991) *Arabidopsis thaliana* as a new model host for plant-parasitic nematodes. *Plant J.* **1**, 245–254.

Smant, G., Helder, J. and Goverse, A. (2018) Parallel adaptations and common host cell responses enabling feeding of obligate and facultative plant parasitic nematodes. *Plant J.* **93**, 686–702.

Sobczak, M., Golinowski, W. and Grundler, F.M.W. (1997) Changes in the structure of *Arabidopsis thaliana* roots induced during development of males of the plant parasitic nematode *Heterodera schachtii*. *Eur. J. Plant Pathol.* **103**, 113–124.

Szakasits, D., Heinen, P., Wieczorek, K., Hofmann, J., Wagner, F., Kreil, D.P., Sykacek, P., Grundler, F.M.W. and Bohlmann, H. (2009) The transcriptome of syncytia induced by the cyst nematode *Heterodera schachtii* in Arabidopsis roots. *Plant J.* **57**, 771–784.

Ursache, R., Andersen, T.G., Marhavý, P. and Geldner, N. (2018) A protocol for combining fluorescent proteins with histological stains for diverse cell wall components. *Plant J.* **93**, 399–412.

Valette, C., Andary, C., Geiger, J.P., Sarah, J.L. and Nicole, M. (1998) Histochemical and cytochemical investigations of phenols in roots of banana infected by the burrowing nematode *Radopholus similis*. *Phytopathology*, **88**, 1141–1148.

Vermeer, J.E.M., von Wangenheim, D., Barberon, M., Lee, Y., Stelzer, E.H.K., Maizel, A. and Geldner, N. (2014) A spatial accommodation by neighboring cells is required for organ initiation in Arabidopsis. *Science*, **343**, 178–183.

Wunderling, A., Ripper, D., Barra-Jimenez, A., Mahn, S., Sajak, K., Ben Targem, M. and Ragni, L. (2018) A molecular framework to study periderm formation in Arabidopsis. *New Phytol.* **219**, 216–229.

Wyss, U. and Grundler, F.M.W. (1992) Feeding behavior of sedentary plant parasitic nematodes. *Neth. J. Plant Pathol.* **98**, 165–173.

Wyss, U., Grundler, F.M.W. and Munch, A. (1992) The parasitic behaviour of second-stage juveniles of *Meloidogyne incognita* in roots of *Arabidopsis thaliana*. *Nematologica*, **38**, 98–111.